First-Principles-Driven Model-Based Optimal Control of the Current Profile in NSTX-U

Zeki Okan Ilhan, William Wehner, Justin Barton, Eugenio Schuster,
David Gates, Stefan Gerhardt, Jonathan Menard

***Abstract*— Regulation in time of the toroidal current profile is one of the main challenges toward the realization of the next-step operational goals for the National Spherical Tokamak eXperiment - Upgrade (NSTX-U). In this work, a nonlinear, control-oriented, physics-based model describing the temporal evolution of the current profile is first obtained by combining the magnetic diffusion equation with empirical correlations obtained for the electron density, electron temperature, and non-inductive current drives in NSTX-U. The proposed model is then embedded into the control design process to synthesize a time-variant, linear-quadratic-integral, optimal controller capable of regulating the safety factor profile around a desired target profile while rejecting disturbances. Neutral beam injectors, electron density, and the total plasma current are used as actuators to shape the current profile. The effectiveness of the proposed controller in regulating the safety factor profile in NSTX-U is demonstrated in closed-loop nonlinear simulations.**

I. Introduction

Conventional nuclear power plants operate based on nuclear fission, which produces energy through the splitting of heavy atoms like uranium. Unfortunately, the by-products of fission are highly radioactive, which require special storage and handling for thousands of years. Unlike fission, nuclear fusion is the process by which two light nuclei (deuterium and tritium) are fused together to form a heavier nucleus (helium) and free a neutron, with energy release as a by-product. The energy released per gram of fuel in a typical fusion reaction is significantly larger than that of a typical fission reaction. Contrary to fission, fusion poses no risk of a nuclear accident, generates no material for nuclear weapons, and produces mostly short-term, low-level, radioactive waste, which can be easily disposed of within a human lifetime [1].

Despite all its benefits, including an abundant fuel supply, achieving controlled fusion on Earth is challenging in the sense that it requires high temperature (10^7-10^9 K) and pressure in order to overcome the so-called Coulomb barrier that prevents the nuclei from fusing together. The high temperature and pressure cause the reactants (hydrogen isotopes) to ionize and enter into the so-called plasma state. The main challenge of nuclear fusion is to confine the hot plasma in order to prevent it from hitting the walls of the confining device. Among several confinement techniques, the tokamak [2] is one of the most promising concepts. The word "tokamak" is the Russian acronym for "toroidal chamber with magnetic coils." A tokamak device exploits the plasma's ability to conduct electrical current and interact with magnetic fields in order to achieve the desired confinement. In a typical tokamak device, the magnetic field produced by both the large magnetic coils around the toroidal chamber and the current flowing toroidally in the plasma describes a helical path through the torus (Fig.1.), i.e., the magnetic field lines curve around in the poloidal direction as well as in the toroidal direction.

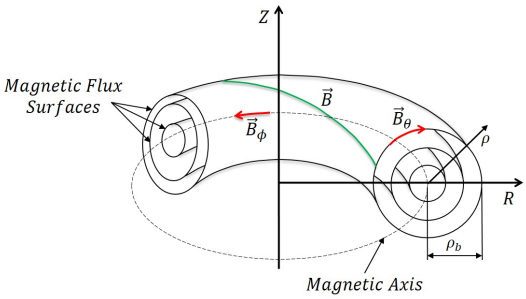

Fig. 1. Magnetic flux surfaces (defined by a constant poloidal magnetic flux) in a tokamak. The helical magnetic field ($\vec{B}$) in a tokamak plasma is composed of toroidal ($\vec{B}_\phi$) and poloidal ($\vec{B}_\theta$) fields. The poloidal magnetic flux is defined as $\Psi = \int \vec{B}_\theta \cdot d\vec{A}_Z$, where $\vec{A}_Z$ denotes a disk of radius R that is perpendicular to a unit vector in the Z direction. The limiting flux surface at the center of the plasma is called the magnetic axis.

A spherical tokamak, or a spherical torus (ST), is a variation of the conventional tokamak concept that utilizes a significantly narrow aspect ratio. Hence, instead of a donut shape, the plasma edge looks almost like a sphere. The ST device is a leading candidate for facilities designed to study plasma material interactions, nuclear component testing, or to generate fusion power. This interest is driven by the compact nature of the ST device and associated excellent utilization of the toroidal field (TF), the natural elongation of the plasma cross-section, the high neutron wall loading, the significantly higher β values (β represents a measure of efficiency of confinement since it defines how much magnetic confining pressure is required to maintain a particular plasma kinetic pressure), and the potential ease of maintenance. The National Spherical Tokamak eXperiment - Upgrade (NSTX-U), depicted in Fig.2, is one of the major ST experimental facilities in the world. NSTX-U is a substantial upgrade to the former NSTX device, with significantly higher toroidal field and solenoid capabilities, and three additional neutral beam sources with significantly larger current-drive efficiency [3].

This work was supported by the U.S. Department of Energy under contract number DE-AC02-09CH11466. Z. O. Ilhan, W. Wehner, J. Barton and E. Schuster are with the Department of Mechanical Engineering and Mechanics, Lehigh University, Bethlehem, PA 18015, USA (e-mail: zoi210@lehigh.edu, schuster@lehigh.edu). D. Gates, S. Gerhardt and J. Menard are with Princeton Plasma Physics Laboratory (PPPL), Princeton, NJ 08544, USA.

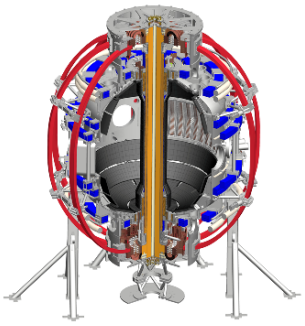

Fig. 2. Schematic of the NSTX-U device in Princeton Plasma Physics Laboratory (PPPL), Princeton, NJ, USA.

The safety factor, q, (defined as the ratio between the number of times a magnetic field line goes toroidally (i.e., the long way) around the tokamak to the number of times it goes around poloidally (i.e., the short way)) is a key property affecting stability, performance, and steady-state operation in fusion plasmas. Therefore, control of the q-profile (q as a function of the plasma coordinate ρ in Fig.1) is important for the realization of these next-step operational goals in NSTX-U. Since the value of q on a flux surface is inversely proportional to the plasma current enclosed by that flux surface, control of the q-profile is equivalent to control of the current profile. In this work, a model-based feedback controller is proposed for the first time to regulate the q-profile in NSTX-U. To facilitate the control design, a nonlinear, control-oriented, physics-based model describing the temporal evolution of the current profile in NSTX-U is first obtained. The proposed model is embedded into the design process to synthesize a time-variant, linear-quadratic-integral, optimal controller. The neutral beam injectors, electron density, and the total plasma current are used as control actuators to manipulate the profile shape. The effectiveness of the proposed controller in shaping the q-profile is shown in closed-loop nonlinear simulations.

II. First-Principles-Driven (FPD) Modeling of the Safety Factor Profile

Any arbitrary quantity that is constant on each magnetic flux surface within the tokamak plasma can be used to index the flux surfaces, which are graphically depicted in Fig. 1. In this work, we choose the mean effective minor radius, ρ, of the flux surface, i.e., $\pi B_{\phi,0}\rho^2 = \Phi$, as the indexing variable, where Φ is the toroidal magnetic flux and $B_{\phi,0}$ is the vacuum toroidal magnetic field at the geometric major radius R_0 of the tokamak. The normalized effective minor radius is defined as $\hat{\rho} = \rho/\rho_b$, where ρ_b is the mean effective minor radius of the last closed flux surface.

In practice, the toroidal current density is usually specified indirectly by the safety factor q, which is in turn related to poloidal magnetic flux Ψ and is defined as $q(\hat{\rho},t) = -d\Phi/d\Psi$. Using $\Phi = \pi B_{\phi,0}\rho^2$ and $\hat{\rho} = \rho/\rho_b$, the q profile is expressed as

$$q(\hat{\rho},t) = -\frac{d\Phi}{d\Psi} = -\frac{d\Phi}{2\pi d\psi} = -\frac{\frac{\partial\Phi}{\partial\rho}\frac{\partial\rho}{\partial\hat{\rho}}}{2\pi\frac{\partial\psi}{\partial\hat{\rho}}} = -\frac{B_{\phi,0}\rho_b^2\hat{\rho}}{\partial\psi/\partial\hat{\rho}}, \quad (1)$$

where the parameter $\psi(\hat{\rho},t)$ is the poloidal stream function, which is closely related to the poloidal flux Ψ ($\Psi = 2\pi\psi$).

The evolution in time of the toroidal current profile in tokamaks is therefore related to the evolution in time of the poloidal magnetic flux profile. The evolution of the poloidal magnetic flux is given in normalized cylindrical coordinates by the magnetic diffusion equation (MDE) [4]:

$$\frac{\partial\psi}{\partial t} = \frac{\eta(T_e)}{\mu_0\rho_b^2\hat{F}^2}\frac{1}{\hat{\rho}}\frac{\partial}{\partial\hat{\rho}}\left(\hat{\rho}D_\psi\frac{\partial\psi}{\partial\hat{\rho}}\right) + R_0\hat{H}\eta(T_e)\frac{\langle\bar{j}_{ni}\cdot\bar{B}\rangle}{B_{\phi,0}}, \quad (2)$$

with boundary conditions

$$\left.\frac{\partial\psi}{\partial\hat{\rho}}\right|_{\hat{\rho}=0} = 0 \qquad \left.\frac{\partial\psi}{\partial\hat{\rho}}\right|_{\hat{\rho}=1} = -\frac{\mu_0}{2\pi}\frac{R_0}{\hat{G}\Big|_{\hat{\rho}=1}\hat{H}\Big|_{\hat{\rho}=1}}I(t), \quad (3)$$

where η is the plasma resistivity, T_e is the electron temperature, μ_0 is the vacuum permeability, $\bar{j}_{ni}$ is any source of noninductive current density, $\bar{B}$ is the magnetic field, $\langle\rangle$ denotes a flux-surface average, $D_\psi(\hat{\rho}) = \hat{F}(\hat{\rho})\hat{G}(\hat{\rho})\hat{H}(\hat{\rho})$, where $\hat{F}$, $\hat{G}$, $\hat{H}$ are geometric factors pertaining to the magnetic configuration of a particular plasma equilibrium, which are functions of $\hat{\rho}$ and $I(t)$ is the total plasma current.

The first-principles model of the poloidal magnetic flux evolution (2) needs to be converted into a form suitable for control design. This is mainly accomplished by combining the poloidal flux evolution model with simplified control-oriented models of the electron density and temperature, the plasma resistivity, and the noninductive current drives [5] tailored to the NSTX-U geometry and actuators. Note that the simplified physics-based models need only to capture the dominant physics that describe how the control actuators affect the respective plasma parameters since feedback control compensates for the modeling uncertainties.

A. Electron Density Modeling

The electron density profile $n_e(\hat{\rho},t)$ is modeled as

$$n_e(\hat{\rho},t) = n_e^{prof}(\hat{\rho})u_n(t), \quad (4)$$

where $n_e^{prof}(\hat{\rho})$ is a reference profile and $u_n(t)$ regulates the time evolution of the electron density. Note that n_e^{prof} is obtained by evaluating the experimental or simulated n_e at a reference time $t_{r_{n_e}}$, i.e., $n_e^{prof}(\hat{\rho}) = n_e(\hat{\rho},t_{r_{n_e}})/u_n(t_{r_{n_e}})$. This model assumes that the control action employed to regulate the electron density weakly affects its radial distribution.

B. Electron Temperature Modeling

The electron temperature $T_e(\hat{\rho},t)$ is modeled as

$$T_e(\hat{\rho},t) = k_{T_e}(\hat{\rho})\frac{T_e^{prof}(\hat{\rho})}{n_e(\hat{\rho},t)}I(t)\sqrt{P_{inj}(t)}, \quad (5)$$

where $P_{inj}(t)$ is the total power injected into the plasma [5], $T_e^{prof}(\hat{\rho})$ is a reference profile obtained at a reference time $t_{r_{T_e}}$, i.e., $T_e^{prof}(\hat{\rho}) = T_e(\hat{\rho},t_{r_{T_e}})$, and $k_{T_e}(\hat{\rho})$ is the electron temperature profile constant evaluated at the reference time, i.e., $k_{T_e}(\hat{\rho}) = n_e(\hat{\rho},t_{r_{T_e}})/[I(t_{r_{T_e}})\sqrt{P_{inj}(t_{r_{T_e}})}]$.

C. Plasma Resistivity Modeling

The resistivity η scales with the electron temperature as

$$\eta(\hat{\rho},t) = k_{sp}(\hat{\rho}) Z_{eff}/[T_e(\hat{\rho},t)^{3/2}], \tag{6}$$

where Z_{eff} is the effective average charge of the ions in the plasma and $k_{sp}(\hat{\rho}) = \eta(\hat{\rho},t_{r_\eta}) T_e(\hat{\rho},t_{r_\eta})^{3/2}/Z_{eff}$ is a constant profile obtained at a reference time t_{r_η}.

D. Noninductive Current-Drive Modeling

The total noninductive current-drive in NSTX-U is produced by the neutral beam injectors and the bootstrap current, and it is expressed as

$$\frac{\langle \bar{j}_{ni} \cdot \bar{B} \rangle}{B_{\phi,0}} = \sum_{i=1}^{6} \frac{\langle \bar{j}_{nbi_i} \cdot \bar{B} \rangle}{B_{\phi,0}} + \frac{\langle \bar{j}_{bs} \cdot \bar{B} \rangle}{B_{\phi,0}}, \tag{7}$$

where $\bar{j}_{nbi_i}$ is the noninductive current generated by the individual neutral beam injectors, and $\bar{j}_{bs}$ is the noninductive current generated by the bootstrap effect [6].

1) Neutral beam Injection Current-Drive: Each auxiliary noninductive current-source is modeled as the time varying power in each actuator multiplied by a deposition profile in space. Therefore, the noninductive current density provided by each individual neutral beam injector is modeled as

$$\frac{\langle \bar{j}_i \cdot \bar{B} \rangle}{B_{\phi,0}}(\hat{\rho},t) = k_i^{prof}(\hat{\rho}) j_i^{dep}(\hat{\rho}) \frac{\sqrt{T_e(\hat{\rho},t)}}{n_e(\hat{\rho},t)} P_i(t), \tag{8}$$

where $i = 1,2,...,6$, $P_i(t)$ represents the neutral beam injection power for each beamline, $k_i^{prof}(\hat{\rho})$ is a normalizing profile, and $j_i^{dep}(\hat{\rho})$ is a reference profile for each current-drive source. Note that $j_i^{dep}(\hat{\rho})$ is obtained at a reference time $t_{r_{nbi}}$, i.e., $j_i^{dep}(\hat{\rho}) = [\langle \bar{j}_i \cdot \bar{B} \rangle / B_{\phi,0}](\hat{\rho}, t_{r_{nbi}})$. The constant profiles k_i^{prof} are expressed as $k_i^{prof}(\hat{\rho}) = n_e(\hat{\rho}, t_{r_{nbi}})/[\sqrt{T_e(\hat{\rho}, t_{r_{nbi}})} P_i(t_{r_{nbi}})]$ and are also evaluated at the reference time $t_{r_{nbi}}$.

2) Bootstrap Current-Drive: Based on [7], the bootstrap current is modeled as

$$\frac{\langle \bar{j}_{bs} \cdot \bar{B} \rangle}{B_{\phi,0}}(\hat{\rho},t) = \frac{k_{JkeV} R_0}{\hat{F}} \left(\frac{\partial \psi}{\partial \hat{\rho}}\right)^{-1} \left[2\mathcal{L}_{31} T_e \frac{\partial n_e}{\partial \hat{\rho}} + \{2\mathcal{L}_{31} + \mathcal{L}_{32} + \alpha \mathcal{L}_{34}\} n_e \frac{\partial T_e}{\partial \hat{\rho}} \right], \tag{9}$$

where $\mathcal{L}_{31}$, $\mathcal{L}_{32}$, $\mathcal{L}_{34}$, and α depend on the magnetic configuration of a particular plasma equilibrium and $k_{JkeV} = 1.602 \times 10^{-16}$ J/keV is the conversion factor from keV to J.

By substituting the simplified scenario-oriented models for the electron density (4), electron temperature (5), plasma resistivity (6), and noninductive current drives (7)-(9) into the MDE (2)-(3), space and time functions can be separated. As a result, the MDE takes the form

$$\frac{\partial \psi}{\partial t} = f_\eta(\hat{\rho}) u_\eta(t) \frac{1}{\hat{\rho}} \frac{\partial}{\partial \hat{\rho}} \left(\hat{\rho} D_\psi(\hat{\rho}) \frac{\partial \psi}{\partial \hat{\rho}} \right) + \sum_{i=1}^{6} f_i(\hat{\rho}) u_i(t) + f_{bs}(\hat{\rho}) u_{bs}(t) \left(\frac{\partial \psi}{\partial \hat{\rho}}\right)^{-1}, \tag{10}$$

with boundary conditions $\frac{\partial \psi}{\partial \hat{\rho}}\Big|_{\hat{\rho}=0} = 0$ and $\frac{\partial \psi}{\partial \hat{\rho}}\Big|_{\hat{\rho}=1} = -f_b I(t)$, where $f_b = [\mu_0 R_0]/[2\pi \hat{G}(1)\hat{H}(1)]$. The spatial functions f_η, f_i, and f_{bs} are dependent on the model profiles, whereas the time functions u_η, u_i, and u_{bs} are the manipulated control inputs expressed as

$$u_\eta(t) = \left[u_n(t)\, I(t)^{-1}\, P_{tot}(t)^{-1/2} \right]^{3/2}, \tag{11}$$

$$u_i(t) = \left[P_i(t)\, I(t)^{-1}\, P_{tot}(t)^{-1/2} \right], \; i = 1,2,...,6, \tag{12}$$

$$u_{bs}(t) = \left[u_n(t)^3\, I(t)^{-1}\, P_{tot}(t)^{-1/2} \right]^{1/2}. \tag{13}$$

Since the safety factor q depends inversely on the poloidal flux gradient (see (1)), it is possible to define $\theta(\hat{\rho},t) = \partial\psi/\partial\hat{\rho}$ as the *to-be-controlled variable*. By differentiating (10) wrt $\hat{\rho}$, the PDE governing the evolution of $\theta(\hat{\rho},t)$ can be written compactly as

$$\frac{\partial \theta}{\partial t} = h_0 u_\eta \theta'' + h_1 u_\eta \theta' + h_2 u_\eta \theta + f'_{bs} \frac{1}{\theta} u_{bs} - f_{bs} \frac{\theta'}{\theta^2} u_{bs} + \sum_{i=1}^{6} f'_i u_i \,, \tag{14}$$

with boundary conditions $\theta\big|_{\hat{\rho}=0} = 0$, $\theta\big|_{\hat{\rho}=1} = -f_b I(t)$, where $(.)' = \partial/\partial\hat{\rho}$ for simplicity, and

$$h_0(\hat{\rho}) = D_\psi(\hat{\rho}) f_\eta(\hat{\rho}), \tag{15}$$

$$h_1(\hat{\rho}) = \left(D'_\psi(\hat{\rho}) + \frac{1}{\hat{\rho}} D_\psi(\hat{\rho}) + D'_\psi(\hat{\rho}) \right) f_\eta(\hat{\rho}) + D_\psi(\hat{\rho}) f'_\eta(\hat{\rho}), \tag{16}$$

$$h_2(\hat{\rho}) = \left(D''_\psi(\hat{\rho}) + \frac{1}{\hat{\rho}} D'_\psi(\hat{\rho}) - \frac{1}{\hat{\rho}^2} D_\psi(\hat{\rho}) \right) f_\eta(\hat{\rho}) + \left(D'_\psi(\hat{\rho}) + \frac{1}{\hat{\rho}} D_\psi(\hat{\rho}) \right) f'_\eta(\hat{\rho}). \tag{17}$$

III. Model Order Reduction and Linearization

A. Model Reduction via Truncated Taylor Series Expansion

To construct a reduced-order model suitable for feedback control, the governing PDE (14) is discretized in space using the truncated Taylor series approach while leaving the time domain continuous. The non-dimensional spatial domain ($\hat{\rho} \in [0,\, 1]$) is divided into l radial nodes, hence, the radial grid size becomes $\Delta\hat{\rho} = 1/(l-1)$. Central finite difference formulae of $O(\Delta\hat{\rho}^2)$ are used to approximate the spatial derivatives for the interior nodes, while forward and backward finite difference approximations of $O(\Delta\hat{\rho}^2)$ are used at the left and right boundary nodes, respectively. Since equation (14) is a non-linear PDE, the discrete form of it yields a set of nonlinear ODEs, which can be represented compactly as

$$\dot{\theta}(t) = g(\theta(t), u(t)), \tag{18}$$

where $\theta = [\theta_2, \theta_3, ..., \theta_{l-1}]^T \in \mathbb{R}^{(l-2)\times 1}$ is the value of $\theta(\hat{\rho},t)$ at the $n = l-2$ interior nodes and $u = [u_\eta, u_1, u_2, ..., u_6, u_{bs}, I]^T \in \mathbb{R}^{9\times 1}$ represents the outputs of the profile controller (manipulated plant inputs) and $g \in \mathbb{R}^{(l-2)\times 1}$ is a nonlinear vector function of the states, inputs, and the model parameters.

B. Model Linearization

Let $u_r(t)$ and $\theta_r(t)$ define a set of inputs and states satisfying the nonlinear, reduced-order model (18), i.e.,

$$\dot{\theta}_r = g(\theta_r, u_r). \tag{19}$$

To obtain a model suitable for control design, we define the following perturbation values

$$\Delta\theta(t) = \theta(t) - \theta_r(t), \qquad \Delta u(t) = u(t) - u_r(t), \tag{20}$$

where $\Delta\theta(t)$ is the deviation from $\theta_r(t)$, and $\Delta u(t)$ is the to-be-designed feedback control. A first-order Taylor series expansion of (18) can be written around θ_r and u_r as

$$\dot{\theta} = g(\theta_r, u_r) + \left.\frac{\partial g}{\partial \theta}\right|_{\theta_r, u_r} (\theta - \theta_r) + \left.\frac{\partial g}{\partial u}\right|_{\theta_r, u_r} (u - u_r). \tag{21}$$

By substituting (20) into (21),

$$\Delta\dot{\theta} + \dot{\theta}_r = g(\theta_r, u_r) + \left.\frac{\partial g}{\partial \theta}\right|_{\theta_r, u_r} \Delta\theta \; + \left.\frac{\partial g}{\partial u}\right|_{\theta_r, u_r} \Delta u, \tag{22}$$

and using (19), it is possible to obtain a Linear, Time-Variant (LTV), state-space model for the perturbation dynamics as

$$\Delta\dot{\theta}(t) = A(t)\Delta\theta(t) + B(t)\Delta u(t)\ , \tag{23}$$

where the system jacobians are expressed compactly as

$$A(t) = \left.\frac{\partial g}{\partial \theta}\right|_{\theta_r(t), u_r(t)}, \qquad B(t) = \left.\frac{\partial g}{\partial u}\right|_{\theta_r(t), u_r(t)}. \tag{24}$$

IV. Control System Structure

In this section, a multi-input-multi-output (MIMO) feedback controller is designed based on the state-space, reduced-order, control-oriented model in its time-variant (LTV) form (23). The control goal is to regulate the evolution of the poloidal magnetic flux gradient profile, and thus the current profile or the safety factor profile, in NSTX-U. The proposed controller is then tested in numerical simulations based on the full magnetic diffusion equation (2).

A. Optimal Tracking Control Problem Statement

In addition to the state equation (23), an output equation can be defined to provide a linear combination of the states. The overall plant is then characterized by the following LTV, MIMO system

$$\Delta\dot{\theta}(t) = A(t)\Delta\theta(t) + B(t)\Delta u(t), \quad y(t) = C\Delta\theta(t), \tag{25}$$

where $C \in \mathbb{R}^{m\times n}$ is the output matrix and $y(t) \in \mathbb{R}^{m\times 1}$ is the output vector with $m = 9$ (number of control outputs chosen equal to the number of control inputs). The role of the matrix C is to select those states, that is, those radial points of the q-profile, where the profile control must be achieved. Hence, each row of C has only one nonzero element, which is equal to one and is located at the column associated with the state to be controlled.

Let $\theta_r(t)$ represent a target magnetic flux gradient profile corresponding to a target q-profile. The tracking problem for $\theta(t)$ then becomes a regulation problem for $\Delta\theta(t)$, since $\Delta\theta(t) = \theta(t) - \theta_r(t)$. Therefore, the control objective is to regulate the output $y(t)$ around zero *as closely as possible* during the time interval $[t_0, t_f]$ with *minimum control effort.* This defines a standard Linear-Quadratic-Regulator (LQR) optimal control problem, the solution of which is in state-feedback form utilizing the time-varying Kalman Gain [8]. To improve the performance of the closed-loop system and reject the effect of possible disturbances, integral action should be added to the optimal control law.

B. Linear-Quadratic-Integral (LQI) Optimal Controller

The LQI optimal control problem is considered here since it adds the desired integral action to the LQR problem. To obtain the LQI controller, a new state variable, $e(t)$ is introduced to be the integral of the output $y(t)$

$$e(t) = \int_{t_0}^{t} y(\tau)\, d\tau = C\int_{t_0}^{t} \Delta\theta(\tau)\, d\tau. \tag{26}$$

The derivative of the integral error (26) then becomes

$$\dot{e}(t) = C\Delta\theta(t). \tag{27}$$

A new, enlarged state variable, $\widetilde{x}(t)$ can be introduced by augmenting the integral error (26) with the actual state $\Delta\theta(t)$, i.e.

$$\widetilde{x}(t) = \begin{bmatrix} e(t) \\ \Delta\theta(t) \end{bmatrix}. \tag{28}$$

Substituting (27) and (25) into (28), the time derivative of the augmented state vector, $\dot{\widetilde{x}}(t)$, becomes

$$\begin{bmatrix} \dot{e}(t) \\ \Delta\dot{\theta}(t) \end{bmatrix} = \begin{bmatrix} 0 & C \\ 0 & A(t) \end{bmatrix} \begin{bmatrix} e(t) \\ \Delta\theta(t) \end{bmatrix} + \begin{bmatrix} 0 \\ B(t) \end{bmatrix} \Delta u(t). \tag{29}$$

Based on (29), the enlarged system can be rewritten compactly as

$$\dot{\widetilde{x}}(t) = \widetilde{A}(t)\widetilde{x}(t) + \widetilde{B}(t)\Delta u(t). \tag{30}$$

To minimize a weighted combination of the tracking error and control energy, one can consider the following standard, quadratic performance index expressed in terms of the enlarged system (30)

$$\begin{aligned} \min_{\Delta u(t)} J =& \frac{1}{2}\widetilde{x}^T(t_f)P(t_f)\widetilde{x}(t_f) \\ &+ \frac{1}{2}\int_{t_0}^{t_f} \left[\widetilde{x}^T(t)Q\widetilde{x}(t) + \Delta u^T(t)R\Delta u(t)\right] dt, \end{aligned} \tag{31}$$

where $P(t_f) \in \mathbb{R}^{(m+n)\times(m+n)}$, $Q \in \mathbb{R}^{(m+n)\times(m+n)}$, and $R \in \mathbb{R}^{m\times m}$ are symmetric, positive definite weight matrices. The solution of the optimal control problem defined by the linear-time-variant plant, (30), and the quadratic performance index, (31), yields a time-variant state-feedback of the form

$$\Delta u(t) = -K(t)\widetilde{x}(t), \tag{32}$$

where $K(t) \in \mathbb{R}^{m\times(m+n)}$ is the *Kalman Gain* given by

$$K(t) = R^{-1}\widetilde{B}^T(t)P(t), \tag{33}$$

and $P(t)$ is the solution of the matrix Riccati Differential Equation (RDE)

$$\begin{aligned} \dot{P}(t) =& -\widetilde{A}^T(t)P(t) - P(t)\widetilde{A}(t) \\ &+ P(t)\widetilde{B}(t)R^{-1}\widetilde{B}^T(t)P(t) - Q, \end{aligned} \tag{34}$$

subject to the final condition $P(t_f)$ [8]. The optimal feedback control law $\Delta u(t)$ for the enlarged system (30) then becomes

$$\Delta u(t) = -K(t)\widetilde{x}(t) = -[K_I(t)\ K_P(t)] \begin{bmatrix} e(t) \\ \Delta\theta(t) \end{bmatrix} = -K_I(t)e(t) - K_P(t)\Delta\theta(t). \quad (35)$$

Finally, substituting the integral error (26) back into (35), the optimal control law can be written as

$$\Delta u(t) = -K_I(t)\int_{t_0}^{t} C\Delta\theta(\tau)d\tau - K_P(t)\Delta\theta(t). \quad (36)$$

Note that the optimal solution (36) yields a PI (Proportional plus Integral) control law.

C. Control Signal Transformation

During the plasma control experiments in NSTX-U and numerical simulations, the outputs of the profile controller $u = [u_\eta, u_1, u_2, u_3, u_4, u_5, u_6, u_{bs}, I(t)]$ need to be converted to the physical actuators, I, P_1, P_2, P_3, P_4, P_5, P_6 and u_n. Inversion of the nonlinear transformations (11)-(13) produce the following expressions for the physical actuators

$$\hat{P}_{tot} = \left(\frac{u_{bs}}{u_\eta I}\right), \quad \hat{P}_1 = u_1 I\sqrt{\hat{P}_{tot}}, \quad \hat{P}_2 = u_2 I\sqrt{\hat{P}_{tot}},$$
$$\hat{P}_3 = u_3 I\sqrt{\hat{P}_{tot}}, \quad \hat{P}_4 = u_4 I\sqrt{\hat{P}_{tot}}, \quad \hat{P}_5 = u_5 I\sqrt{\hat{P}_{tot}},$$
$$\hat{P}_6 = u_6 I\sqrt{\hat{P}_{tot}}, \quad \hat{u}_n = u_{bs}u_\eta^{-1/3}. \quad (37)$$

Note however that the inverse transformations (37) along with the constraint $\hat{P}_{tot} = \hat{P}_1 + \hat{P}_2 + \hat{P}_3 + \hat{P}_4 + \hat{P}_5 + \hat{P}_6$ form a set of over-constrained equations, all of which cannot be satisfied simultaneously. To determine the beam power requests (i.e., P vector in Fig. 3), one needs to solve the best approximation to the over-determined system:

$$X_{LS}\underbrace{[P_1\ P_2\ P_3\ P_4\ P_5\ P_6]^T}_{P_{\text{req}}} = \underbrace{\left[\hat{P}_1\ \hat{P}_2\ \hat{P}_3\ \hat{P}_4\ \hat{P}_5\ \hat{P}_6\ \hat{P}_{\text{tot}}\right]^T}_{\hat{P}} \quad (38)$$

where P_{req} represents the actuator power requests to be determined. The 7 by 6 matrix X_{LS} is defined as $X_{LS}^T = [I_6\ \ \mathbf{1}]$ where I_6 denotes a 6 by 6 identity matrix and $\mathbf{1}$ represents an additional column of ones. The solution of (38) requires solving the minimization problem

$$P_{\text{req}} = \arg\min_{P_{\text{req}}} \left(\hat{P} - X_{LS}P_{\text{req}}\right)^T Q_{LS}\left(\hat{P} - X_{LS}P_{\text{req}}\right), \quad (39)$$

where Q_{LS} is a diagonal weighting matrix. The solution can be written as $P_{req} = (Q_{LS}X_{LS})^+ Q_{LS}\hat{P}$, where the superscript $^+$ denotes the pseudoinverse.

The block diagram in Fig. 3 summarizes the closed-loop LQI control scheme for NSTX-U. T refers to the nonlinear input transformations (11)-(13). The block T^{-1} refers to the the nonlinearity inversion (37)-(39) carried out to determine the actuator power requests. The saturation block and the anti-windup controller are also depicted in Fig. 3.

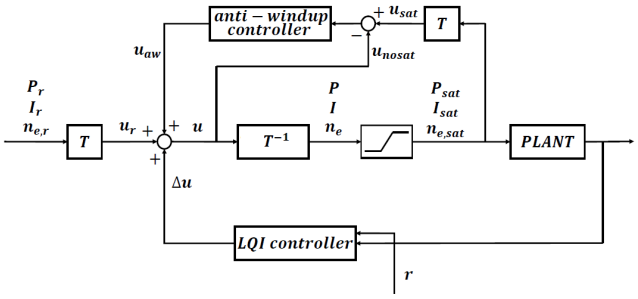

Fig. 3. Closed-loop LQI control scheme showing the nonlinear control signal transformation.

V. Simulation Results

The controller is designed based on the LTV state-space model (23) tailored for NSTX-U. There is no experimental data available yet for NSTX-U since the machine is still undergoing an important upgrade. The model reference profiles and constants are adopted based on numerical predictions by TRANSP, which is a numerical code for predictive tokamak analysis. NSTX-U TRANSP run 121123R42 [3] has been selected for model tailoring since it is a TRANSP run with the NSTX-U shape and actuators, but using scaled profiles from NSTX. The designed controller is tested in closed-loop simulations based on the nonlinear MDE (2)-(3).

The target state trajectory $\theta_r(\hat{\rho}, t)$ is generated by simulating the MDE (2)-(3) with the physical inputs set to arbitrary constants. Both for control design and closed-loop simulation, the non-dimensional spatial domain ($\hat{\rho} \in [0\ 1]$) is divided into $l = 21$ radial nodes, hence, the radial grid size is $\Delta\hat{\rho} = 0.05$. Control simulations are then carried out for $t \in [t_0\ t_f] = [0.1\ 5]$ s. (typical discharge duration expected for NSTX-U). The sampling time is set to $T_s = 0.05$ s.

The tuning of the proposed LQI optimal controller (36) involves the selection of the weight matrices Q and R, whose ratio defines how the trade-off between speed of response and consumption of control energy is weighted. Since the inputs are normalized and the states have the same order of magnitude, both Q and R are selected as diagonal matrices, each having identical diagonal entries. The terminal cost matrix $P(t_f)$ in (31) is set to identity to ensure the tracking error at the final time t_f is equally weighted for all states.

In this closed-loop control simulation study, the initial condition perturbation rejection capability is tested during the first 2 seconds of the discharge by setting $\theta(t_0) = \theta_r(t_0) + \delta\theta$. In addition to an initial condition perturbation, step disturbances are also added in each input channel starting at $t =$ 2s, i.e., $u(t) = \Delta u(t) + u_r(t) + u_d$, $t >$ 2s, where u_d stands for the constant disturbance inputs (0.25 MA for the plasma current, 0.1 MW for each neutral beam injection power, and 0.3 for the electron density regulation). The controller is tuned by setting the ratio between Q and R to 10000, seeking in this way a faster response. The time evolution of the optimal physical inputs are illustrated in Figs. 4(a)-(c). The corresponding time evolution of the optimal outputs are depicted in Fig. 4(d) along with their respective targets. Note from Fig. 4(d) that the states jump again at $t = 2$ s.,

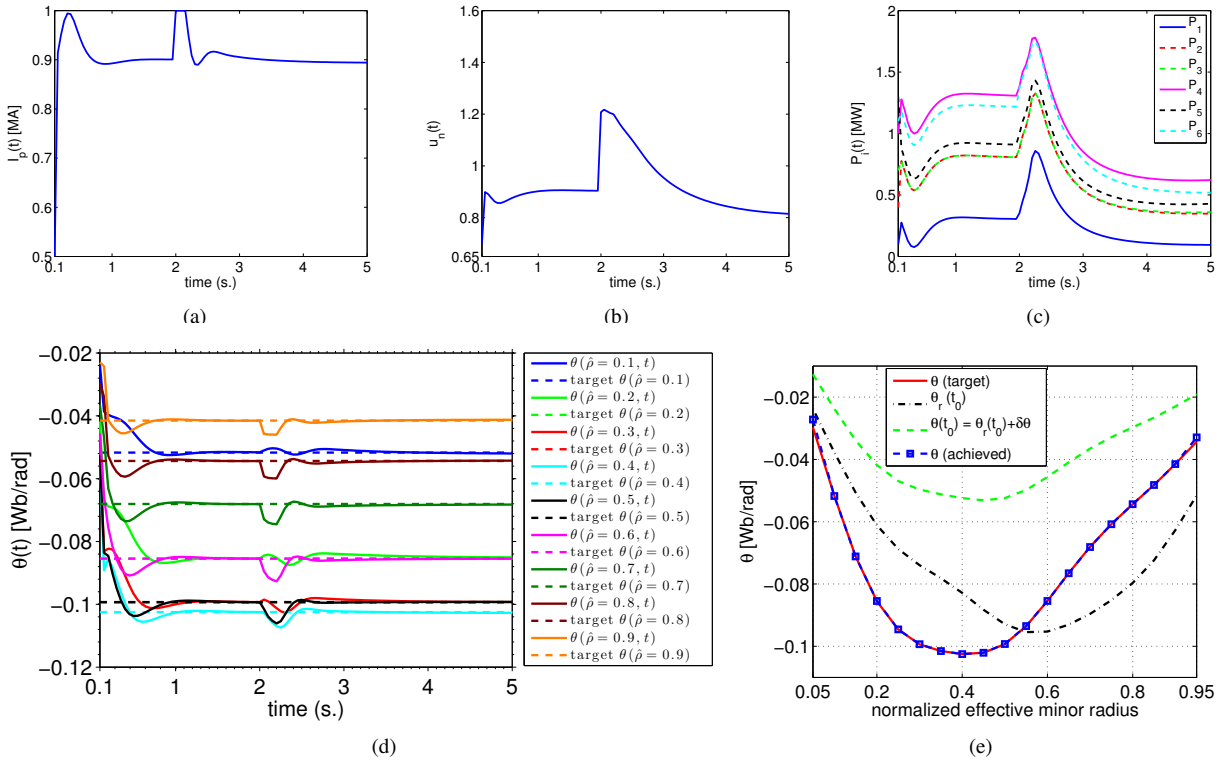

Fig. 4. Tracking simulation results: (a)-(c) Time evolution of the optimal plasma current, electron density regulation and neutral beam injection powers; (d) Time evolution of the optimal outputs (solid) with their respective targets (dashed); (e) Comparison of the initial and desired $\theta(\hat{\rho})$ profiles along with the profile achieved by feedback control at $t = 5$ s.

which is the effect of the step disturbance inputs added at that instant. Fig. 4(e) compares the $\theta(\hat{\rho})$ profile achieved at $t = 5$ s. with the desired target profile along with the actual (unperturbed) initial profile, $\theta_r(t_0)$, and the perturbed initial profile, $\theta(t_0)$. While Fig. 4(e) shows that the desired target profile is achieved at $t = 5$ s., an excellent profile matching is already achieved well before $t = 5$ s. as can be seen from Fig. 4(d). Finally, the time evolution of the corresponding safety factor (q-profile) is shown in Fig. 5 along with the respective initial and target profiles. Based on this simulation analysis, the proposed controller is shown to be effective in regulating the q-profile around a target profile in NSTX-U.

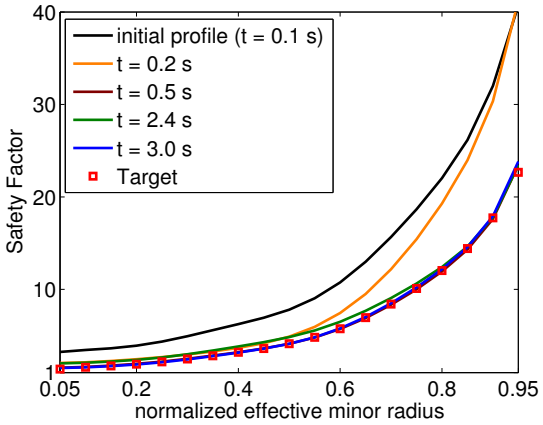

Fig. 5. Time evolution of the safety factor (q-profile).

VI. Conclusion and Future Work

In this work, an NSTX-U-tailored plasma response model is first written in a control-oriented form. The resulting infinite dimensional, nonlinear PDE is then reduced through spatial discretization by a truncated Taylor series expansion. The nonlinear, finite-dimensional model is finally linearized around the target state and input trajectories. An LQI feedback controller is designed based on the resulting LTV model to regulate the poloidal flux gradient profile, and hence the current profile or the safety factor profile, around a desired target profile. The effectiveness of the proposed controller is tested in numerical simulations based on an MDE solver. The main contribution of this work resides in the application itself since this is the first current profile controller ever designed for NSTX-U. The next step is to experimentally test the controller once NSTX-U starts operation.

References

[1] A. Pironti and M. Walker, "Fusion, Tokamaks, and Plasma Control," *IEEE Control Systems Magazine*, vol. 25, no. 5, pp. 30–43, 2005.

[2] J. Wesson, *Tokamaks*. Clarendon Press, Oxford, UK, 1984.

[3] S. P. Gerhardt, R. Andre, and J. E. Menard, "Exploration of the equilibrium operating space for NSTX-Upgrade," *Nuclear Fusion*, vol. 52, no. 8, 2012.

[4] Y. Ou *et al.*, "Towards model-based current profile control at DIII-D," *Fusion Engineering and Design*, vol. 82, pp. 1153–1160, 2007.

[5] J. E. Barton *et al.*, "Physics-based Control-oriented Modeling of the Safety Factor Profile Dynamics in High Performance Tokamak Plasmas," *52nd IEEE CDC*, pp. 4182–4187, 2013.

[6] A. G. Peeters, "The Bootstrap Current and Its Consequences," *Plasma Phys. and Control. Fusion*, vol. 42, pp. B231–B242, 2000.

[7] O. Sauter *et al.*, "Neoclassical Conductivity and Bootstrap Current Formulas for General Axisymmetric Equilibria and Arbitrary Collisionality Regime," *Physics of Plasmas*, vol. 6, no. 7, p. 2834, 1999.

[8] D. S. Naidu, *Optimal Control Systems*. CRC Press, 2002.